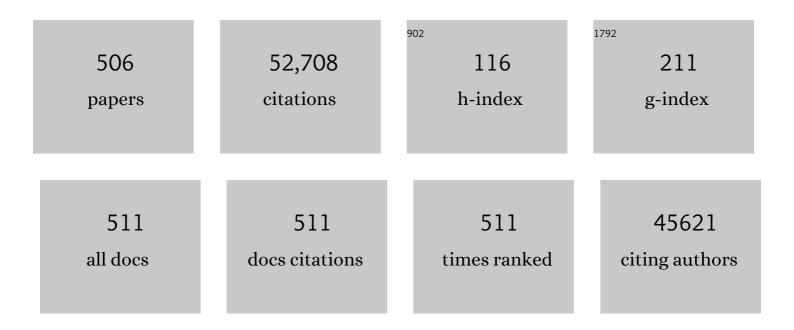
List of Publications by Year in descending order

Source: https://exaly.com/author-pdf/5049431/publications.pdf Version: 2024-02-01



#	Article	IF	CITATIONS
1	Effects of high-temperature CeO ₂ calcination on the activity of Pt/CeO ₂ catalysts for oxidation of unburned hydrocarbon fuels. Catalysis Science and Technology, 2022, 12, 2462-2470.	2.1	5
2	Sulfone-based electrolytes for high energy density lithium-ion batteries. Journal of Power Sources, 2022, 527, 231171.	4.0	21
3	Facile Dual-Protection Layer and Advanced Electrolyte Enhancing Performances of Cobalt-free/Nickel-rich Cathodes in Lithium-Ion Batteries. ACS Applied Materials & Interfaces, 2022, 14, 17405-17414.	4.0	8
4	Bimetallic Ir _{<i>x</i>} Pb nanowire networks with enhanced electrocatalytic activity for the oxygen evolution reaction. Journal of Materials Chemistry A, 2022, 10, 11196-11204.	5.2	6
5	A freeze-thaw molten salt battery for seasonal storage. Cell Reports Physical Science, 2022, 3, 100821.	2.8	5
6	Interfacial Engineering with a Nanoparticle-Decorated Porous Carbon Structure on β″-Alumina Solid-State Electrolytes for Molten Sodium Batteries. ACS Applied Materials & Interfaces, 2022, 14, 25534-25544.	4.0	8
7	Preface for the special topic collection honoring Dr. Scott Chambers' 70th birthday and his leadership in the science and technology of oxide thin films. Journal of Vacuum Science and Technology A: Vacuum, Surfaces and Films, 2022, 40, .	0.9	0
8	Low-solvation electrolytes for high-voltage sodium-ion batteries. Nature Energy, 2022, 7, 718-725.	19.8	137
9	Enhancing Moisture Stability of Sulfide Solid-State Electrolytes by Reversible Amphipathic Molecular Coating. ACS Applied Materials & Interfaces, 2022, 14, 32035-32042.	4.0	5
10	Effects of Fluorinated Diluents in Localized Highâ€Concentration Electrolytes for Lithium–Oxygen Batteries. Advanced Functional Materials, 2021, 31, 2002927.	7.8	39
11	Optimization of fluorinated orthoformate based electrolytes for practical high-voltage lithium metal batteries. Energy Storage Materials, 2021, 34, 76-84.	9.5	65
12	Understanding the Deactivation of Agâ^'ZrO ₂ /SiO ₂ Catalysts for the Singleâ€step Conversion of Ethanol to Butenes. ChemCatChem, 2021, 13, 999-1008.	1.8	11
13	An Ionâ€Imprinting Derived Strategy to Synthesize Singleâ€Atom Iron Electrocatalysts for Oxygen Reduction. Small, 2021, 17, e2004454.	5.2	52
14	High performance sodium-sulfur batteries at low temperature enabled by superior molten Na wettability. Chemical Communications, 2021, 57, 45-48.	2.2	19
15	Rational Design of Electrolytes for Long-Term Cycling of Si Anodes over a Wide Temperature Range. ACS Energy Letters, 2021, 6, 387-394.	8.8	58
16	Molecular Iodine Interactions with Fe, Ni, Cr, and Stainless Steel Alloys. Industrial & Engineering Chemistry Research, 2021, 60, 2447-2454.	1.8	5
17	Effects of fluorinated solvents on electrolyte solvation structures and electrode/electrolyte interphases for lithium metal batteries. Proceedings of the National Academy of Sciences of the United States of America, 2021, 118, .	3.3	131
18	Conversion of ethanol to 1,3–butadiene over Ag–ZrO2/SiO2 catalysts: The role of surface interfaces. Journal of Energy Chemistry, 2021, 54, 7-15.	7.1	21

4

#	Article	IF	CITATIONS
19	Introduction to topical collection: Reproducibility challenges and solutions with a focus on guides to XPS analysis. Journal of Vacuum Science and Technology A: Vacuum, Surfaces and Films, 2021, 39, .	0.9	35
20	Electrolyte Regulating toward Stabilization of Cobalt-Free Ultrahigh-Nickel Layered Oxide Cathode in Lithium-Ion Batteries. ACS Energy Letters, 2021, 6, 1324-1332.	8.8	53
21	Advanced Lowâ€Flammable Electrolytes for Stable Operation of Highâ€Voltage Lithiumâ€Ion Batteries. Angewandte Chemie, 2021, 133, 13109-13116.	1.6	16
22	Advanced Lowâ€Flammable Electrolytes for Stable Operation of Highâ€Voltage Lithiumâ€Ion Batteries. Angewandte Chemie - International Edition, 2021, 60, 12999-13006.	7.2	70
23	Stabilizing ultrahigh-nickel layered oxide cathodes for high-voltage lithium metal batteries. Materials Today, 2021, 44, 15-24.	8.3	53
24	Optimization of Magnesiumâ€Đoped Lithium Metal Anode for High Performance Lithium Metal Batteries through Modeling and Experiment. Angewandte Chemie, 2021, 133, 16642-16649.	1.6	5
25	Polyacrylonitrile Composites of Ag–Al–Si–O Aerogels and Xerogels as Iodine and Iodide Sorbents. ACS Applied Polymer Materials, 2021, 3, 3344-3353.	2.0	11
26	Optimization of Magnesiumâ€Đoped Lithium Metal Anode for High Performance Lithium Metal Batteries through Modeling and Experiment. Angewandte Chemie - International Edition, 2021, 60, 16506-16513.	7.2	28
27	A Polymer-in-Salt Electrolyte with Enhanced Oxidative Stability for Lithium Metal Polymer Batteries. ACS Applied Materials & Interfaces, 2021, 13, 31583-31593.	4.0	28
28	Elucidating the Active Site and the Role of Alkali Metals in Selective Hydrodeoxygenation of Phenols over Ironâ€Carbideâ€based Catalyst. ChemSusChem, 2021, 14, 4546-4555.	3.6	8
29	Tailoring the Local Environment of Platinum in Singleâ€Atom Pt ₁ /CeO ₂ Catalysts for Robust Lowâ€Temperature CO Oxidation. Angewandte Chemie, 2021, 133, 26258-26266.	1.6	7
30	Toward the Practical Use of Cobalt-Free Lithium-Ion Batteries by an Advanced Ether-Based Electrolyte. ACS Applied Materials & Interfaces, 2021, 13, 44339-44347.	4.0	24
31	Tailoring the Local Environment of Platinum in Singleâ€Atom Pt ₁ /CeO ₂ Catalysts for Robust Lowâ€Temperature CO Oxidation. Angewandte Chemie - International Edition, 2021, 60, 26054-26062.	7.2	84
32	Atomic Force Microscopy and Infrared Nanospectroscopy of COVID-19 Spike Protein for the Quantification of Adhesion to Common Surfaces. Langmuir, 2021, 37, 12089-12097.	1.6	5
33	Selective Removal of Perfluorobutyric Acid Using an Electroactive Ion Exchanger Based on Polypyrrole@Iron Oxide on Carbon Cloth. ACS Applied Materials & Interfaces, 2021, 13, 48500-48507.	4.0	8
34	An Electrochemically Activated Nanofilm for Sustainable Mg Anode with Fast Charge Transfer Kinetics. Journal of the Electrochemical Society, 2021, 168, 120519.	1.3	2
35	The Influence of Transitional Metal Dopants on Reducing Chlorine Evolution during the Electrolysis of Raw Seawater. Applied Sciences (Switzerland), 2021, 11, 11911.	1.3	3

Preparation of nanoparticles for surface analysis. , 2020, , 295-347.

#	Article	IF	CITATIONS
37	Correlative surface imaging reveals chemical signatures for bacterial hotspots on plant roots. Analyst, The, 2020, 145, 393-401.	1.7	15
38	Stabilization of Super Electrophilic Pd ⁺² Cations in Small-Pore SSZ-13 Zeolite. Journal of Physical Chemistry C, 2020, 124, 309-321.	1.5	67
39	Reversible Electrochemical Interface of Mg Metal and Conventional Electrolyte Enabled by Intermediate Adsorption. ACS Energy Letters, 2020, 5, 200-206.	8.8	44
40	Enabling Natural Graphite in Highâ€Voltage Aqueous Graphite Zn Metal Dualâ€Ion Batteries. Advanced Energy Materials, 2020, 10, 2001256.	10.2	43
41	Unravelling high-temperature stability of lithium-ion battery with lithium-rich oxide cathode in localized high-concentration electrolyte. Journal of Power Sources Advances, 2020, 5, 100024.	2.6	23
42	Introductory guide to backgrounds in XPS spectra and their impact on determining peak intensities. Journal of Vacuum Science and Technology A: Vacuum, Surfaces and Films, 2020, 38, .	0.9	62
43	Holeâ€Trappingâ€Induced Stabilization of Ni ^{4 +} in SrNiO ₃ /LaFeO ₃ Superlattices. Advanced Materials, 2020, 32, e2005003.	11.1	26
44	Controlling Ion Coordination Structure and Diffusion Kinetics for Optimized Electrode-Electrolyte Interphases and High-Performance Si Anodes. Chemistry of Materials, 2020, 32, 8956-8964.	3.2	24
45	Single-Step Conversion of Ethanol to <i>n</i> -Butene over Ag-ZrO ₂ /SiO ₂ Catalysts. ACS Catalysis, 2020, 10, 10602-10613.	5.5	34
46	Enabling Ether-Based Electrolytes for Long Cycle Life of Lithium-Ion Batteries at High Charge Voltage. ACS Applied Materials & Interfaces, 2020, 12, 54893-54903.	4.0	35
47	A Highâ€Performance Na–Al Battery Based on Reversible NaAlCl ₄ Catholyte. Advanced Energy Materials, 2020, 10, 2001378.	10.2	18
48	Reply to: "Pitfalls in identifying active catalyst species― Nature Communications, 2020, 11, 4574.	5.8	0
49	Highly Reversible Sodium Ion Batteries Enabled by Stable Electrolyte-Electrode Interphases. ACS Energy Letters, 2020, 5, 3212-3220.	8.8	97
50	Performance enhancement and degradation mechanism identification of a single-atom Co–N–C catalyst for proton exchange membrane fuel cells. Nature Catalysis, 2020, 3, 1044-1054.	16.1	443
51	Role of inner solvation sheath within salt–solvent complexes in tailoring electrode/electrolyte interphases for lithium metal batteries. Proceedings of the National Academy of Sciences of the United States of America, 2020, 117, 28603-28613.	3.3	191
52	Designing Advanced In Situ Electrode/Electrolyte Interphases for Wide Temperature Operation of 4.5 V Li LiCoO ₂ Batteries. Advanced Materials, 2020, 32, e2004898.	11.1	123
53	XPS guide: Charge neutralization and binding energy referencing for insulating samples. Journal of Vacuum Science and Technology A: Vacuum, Surfaces and Films, 2020, 38, .	0.9	114
54	Surface engineering of earth-abundant Fe catalysts for selective hydrodeoxygenation of phenolics in liquid phase. Chemical Science, 2020, 11, 5874-5880.	3.7	19

#	Article	IF	CITATIONS
55	Optimized Electrolyte with High Electrochemical Stability and Oxygen Solubility for Lithium–Oxygen and Lithium–Air Batteries. ACS Energy Letters, 2020, 5, 2182-2190.	8.8	45
56	Defect-induced anisotropic surface reactivity and ion transfer processes of anatase nanoparticles. Materials Today Chemistry, 2020, 17, 100290.	1.7	0
57	Dynamic Lattice Oxygen Participation on Perovskite LaNiO ₃ during Oxygen Evolution Reaction. Journal of Physical Chemistry C, 2020, 124, 15386-15390.	1.5	49
58	Sweeping potential regulated structural and chemical evolution of solid-electrolyte interphase on Cu and Li as revealed by cryo-TEM. Nano Energy, 2020, 76, 105040.	8.2	16
59	Size Dependence of Lattice Parameter and Electronic Structure in CeO ₂ Nanoparticles. Inorganic Chemistry, 2020, 59, 5760-5767.	1.9	90
60	A lithium-sulfur battery with a solution-mediated pathway operating under lean electrolyte conditions. Nano Energy, 2020, 76, 105041.	8.2	25
61	In situ molecular imaging of adsorbed protein films in water indicating hydrophobicity and hydrophilicity. Scientific Reports, 2020, 10, 3695.	1.6	10
62	Proliferation of Faulty Materials Data Analysis in the Literature. Microscopy and Microanalysis, 2020, 26, 1-2.	0.2	59
63	Controlling Surface Phase Transition and Chemical Reactivity of O3-Layered Metal Oxide Cathodes for High-Performance Na-Ion Batteries. ACS Energy Letters, 2020, 5, 1718-1725.	8.8	64
64	Excellent Cycling Stability of Sodium Anode Enabled by a Stable Solid Electrolyte Interphase Formed in Etherâ€Based Electrolytes. Advanced Functional Materials, 2020, 30, 2001151.	7.8	60
65	Advanced Electrolytes for Fastâ€Charging Highâ€Voltage Lithiumâ€Ion Batteries in Wideâ€Temperature Range. Advanced Energy Materials, 2020, 10, 2000368.	10.2	159
66	Effect of Cr(III) Adsorption on the Dissolution of Boehmite Nanoparticles in Caustic Solution. Environmental Science & Technology, 2020, 54, 6375-6384.	4.6	8
67	Sequential Ammonia and Carbon Dioxide Adsorption on Pyrolyzed Biomass to Recover Waste Stream Nutrients. ACS Sustainable Chemistry and Engineering, 2020, 8, 7121-7131.	3.2	15
68	Calcareous organic matter coatings sequester siderophores in alkaline soils. Science of the Total Environment, 2020, 724, 138250.	3.9	14
69	X-ray photoelectron spectroscopy data from lightly Pd doped TiO2 anatase nanoparticles. Surface Science Spectra, 2020, 27, .	0.3	4
70	Applications of XPS in the characterization of Battery materials. Journal of Electron Spectroscopy and Related Phenomena, 2019, 231, 2-10.	0.8	101
71	Electrocatalytic Hydrogen Evolution in Neutral pH Solutions: Dual-Phase Synergy. ACS Catalysis, 2019, 9, 8712-8718.	5.5	103
72	Edge Dislocations Induce Improved Photocatalytic Efficiency of Colored TiO ₂ . Advanced Materials Interfaces, 2019, 6, 1901121.	1.9	30

#	Article	IF	CITATIONS
73	Role of Inorganic Surface Layer on Solid Electrolyte Interphase Evolution at Li-Metal Anodes. ACS Applied Materials & Interfaces, 2019, 11, 31467-31476.	4.0	75
74	Highâ€Performance Silicon Anodes Enabled By Nonflammable Localized Highâ€Concentration Electrolytes. Advanced Energy Materials, 2019, 9, 1900784.	10.2	175
75	Enabling High-Voltage Lithium-Metal Batteries under Practical Conditions. Joule, 2019, 3, 1662-1676.	11.7	598
76	Polymerâ€inâ€â€œQuasiâ€lonic Liquid―Electrolytes for Highâ€Voltage Lithium Metal Batteries. Advanced Energ Materials, 2019, 9, 1902108.	^{gy} 10.2	65
77	Origin of lithium whisker formation and growth under stress. Nature Nanotechnology, 2019, 14, 1042-1047.	15.6	211
78	Structure Sensitivity of Acetylene Semi-Hydrogenation on Pt Single Atoms and Subnanometer Clusters. ACS Catalysis, 2019, 9, 11030-11041.	5.5	111
79	Cr(III) Adsorption by Cluster Formation on Boehmite Nanoplates in Highly Alkaline Solution. Environmental Science & Technology, 2019, 53, 11043-11055.	4.6	42
80	Monolithic solid–electrolyte interphases formed in fluorinated orthoformate-based electrolytes minimize Li depletion and pulverization. Nature Energy, 2019, 4, 796-805.	19.8	621
81	Nonflammable Electrolytes for Lithium Ion Batteries Enabled by Ultraconformal Passivation Interphases. ACS Energy Letters, 2019, 4, 2529-2534.	8.8	112
82	A comparative study of pomegranate Sb@C yolk–shell microspheres as Li and Na-ion battery anodes. Nanoscale, 2019, 11, 348-355.	2.8	45
83	Electrically Switched Ion Exchange Based on Carbon-Polypyrrole Composite Smart Materials for the Removal of ReO ₄ [–] from Aqueous Solutions. Environmental Science & Technology, 2019, 53, 2612-2617.	4.6	26
84	Joint Charge Storage for Highâ€Rate Aqueous Zinc–Manganese Dioxide Batteries. Advanced Materials, 2019, 31, e1900567.	11.1	299
85	Constructing Robust Electrode/Electrolyte Interphases to Enable Wide Temperature Applications of Lithium-Ion Batteries. ACS Applied Materials & amp; Interfaces, 2019, 11, 21496-21505.	4.0	44
86	Tuning Pt-CeO2 interactions by high-temperature vapor-phase synthesis for improved reducibility of lattice oxygen. Nature Communications, 2019, 10, 1358.	5.8	302
87	High-Concentration Ether Electrolytes for Stable High-Voltage Lithium Metal Batteries. ACS Energy Letters, 2019, 4, 896-902.	8.8	302
88	Practical guides for x-ray photoelectron spectroscopy: First steps in planning, conducting, and reporting XPS measurements. Journal of Vacuum Science and Technology A: Vacuum, Surfaces and Films, 2019, 37, .	0.9	137
89	Highly Stable Oxygen Electrodes Enabled by Catalyst Redistribution through an In Situ Electrochemical Method. Advanced Energy Materials, 2019, 9, 1803598.	10.2	6
90	Steam reforming of simulated bio-oil on K-Ni-Cu-Mg-Ce-O/Al2O3: The effect of K. Catalysis Today, 2019, 323, 183-190.	2.2	19

#	Article	IF	CITATIONS
91	Surface speciation and interactions between adsorbed chloride and water on cerium dioxide. Journal of Solid State Chemistry, 2018, 262, 16-25.	1.4	5
92	Addressing Passivation in Lithium–Sulfur Battery Under Lean Electrolyte Condition. Advanced Functional Materials, 2018, 28, 1707234.	7.8	143
93	Stability of polymeric separators in lithium metal batteries in a low voltage environment. Journal of Materials Chemistry A, 2018, 6, 5006-5015.	5.2	31
94	Core–shell PdPb@Pd aerogels with multiply-twinned intermetallic nanostructures: facile synthesis with accelerated gelation kinetics and their enhanced electrocatalytic properties. Journal of Materials Chemistry A, 2018, 6, 7517-7521.	5.2	49
95	Synthesis of nanometer-sized fayalite and magnesium-iron(II) mixture olivines. Journal of Colloid and Interface Science, 2018, 515, 129-138.	5.0	19
96	Dendriteâ€Free and Performanceâ€Enhanced Lithium Metal Batteries through Optimizing Solvent Compositions and Adding Combinational Additives. Advanced Energy Materials, 2018, 8, 1703022.	10.2	123
97	Porous Carbonâ€Hosted Atomically Dispersed Iron–Nitrogen Moiety as Enhanced Electrocatalysts for Oxygen Reduction Reaction in a Wide Range of pH. Small, 2018, 14, e1703118.	5.2	117
98	Nitrogenâ€Coordinated Single Cobalt Atom Catalysts for Oxygen Reduction in Proton Exchange Membrane Fuel Cells. Advanced Materials, 2018, 30, 1706758.	11.1	788
99	Effects of Imide–Orthoborate Dual-Salt Mixtures in Organic Carbonate Electrolytes on the Stability of Lithium Metal Batteries. ACS Applied Materials & Interfaces, 2018, 10, 2469-2479.	4.0	110
100	Enhanced Cyclability of Lithium–Oxygen Batteries with Electrodes Protected by Surface Films Induced via In Situ Electrochemical Process. Advanced Energy Materials, 2018, 8, 1702340.	10.2	38
101	The effect of ion irradiation on the dissolution of UO2 and UO2-based simulant fuel. Journal of Alloys and Compounds, 2018, 735, 1350-1356.	2.8	12
102	Enhanced Stability of Lithium Metal Anode by using a 3D Porous Nickel Substrate. ChemElectroChem, 2018, 5, 761-769.	1.7	58
103	Extremely Stable Sodium Metal Batteries Enabled by Localized High-Concentration Electrolytes. ACS Energy Letters, 2018, 3, 315-321.	8.8	373
104	Simultaneous Stabilization of LiNi _{0.76} Mn _{0.14} Co _{0.10} O ₂ Cathode and Lithium Metal Anode by Lithium Bis(oxalato)borate as Additive. ChemSusChem, 2018, 11, 2211-2220.	3.6	89
105	High Voltage Operation of Niâ€Rich NMC Cathodes Enabled by Stable Electrode/Electrolyte Interphases. Advanced Energy Materials, 2018, 8, 1800297.	10.2	298
106	Ultrathin dendritic IrTe nanotubes for an efficient oxygen evolution reaction in a wide pH range. Journal of Materials Chemistry A, 2018, 6, 8855-8859.	5.2	54
107	Highâ€Voltage Lithiumâ€Metal Batteries Enabled by Localized Highâ€Concentration Electrolytes. Advanced Materials, 2018, 30, e1706102.	11.1	761
108	A perspective on two chemometrics tools: PCA and MCR, and introduction of a new one: Pattern recognition entropy (PRE), as applied to XPS and ToF-SIMS depth profiles of organic and inorganic materials. Applied Surface Science, 2018, 433, 994-1017.	3.1	36

#	Article	IF	CITATIONS
109	Ultrafine and highly disordered Ni2Fe1 nanofoams enabled highly efficient oxygen evolution reaction in alkaline electrolyte. Nano Energy, 2018, 44, 319-326.	8.2	118
110	Behavior of Lithium Metal Anodes under Various Capacity Utilization and High Current Density in Lithium Metal Batteries. Joule, 2018, 2, 110-124.	11.7	280
111	Guided Lithium Metal Deposition and Improved Lithium Coulombic Efficiency through Synergistic Effects of LiAsF ₆ and Cyclic Carbonate Additives. ACS Energy Letters, 2018, 3, 14-19.	8.8	161
112	Freestanding NiFe Oxyfluoride Holey Film with Ultrahigh Volumetric Capacitance for Flexible Asymmetric Supercapacitors. Small, 2018, 14, 1702295.	5.2	34
113	Detrimental Effects of Chemical Crossover from the Lithium Anode to Cathode in Rechargeable Lithium Metal Batteries. ACS Energy Letters, 2018, 3, 2921-2930.	8.8	89
114	Cr(VI) Effect on Tc-99 Removal from Hanford Low-Activity Waste Simulant by Ferrous Hydroxide. Environmental Science & Technology, 2018, 52, 11752-11759.	4.6	11
115	Decorating β′′-alumina solid-state electrolytes with micron Pb spherical particles for improving Na wettability at lower temperatures. Journal of Materials Chemistry A, 2018, 6, 19703-19711.	5.2	44
116	The Effect of Solvent on the Capacity Retention in a Germanium Anode for Lithium Ion Batteries. Journal of Electrochemical Energy Conversion and Storage, 2018, 15, .	1.1	4
117	High-Efficiency Lithium Metal Batteries with Fire-Retardant Electrolytes. Joule, 2018, 2, 1548-1558.	11.7	436
118	Structural identification of ZnxZryOz catalysts for Cascade aldolization and self-deoxygenation reactions. Applied Catalysis B: Environmental, 2018, 234, 337-346.	10.8	43
119	Lithiumâ€Metal Batteries: Highâ€Voltage Lithiumâ€Metal Batteries Enabled by Localized Highâ€Concentration Electrolytes (Adv. Mater. 21/2018). Advanced Materials, 2018, 30, 1870144.	11.1	4
120	Self-organizing layers from complex molecular anions. Nature Communications, 2018, 9, 1889.	5.8	43
121	Lithiumâ€Pretreated Hard Carbon as Highâ€Performance Sodiumâ€ŀon Battery Anodes. Advanced Energy Materials, 2018, 8, 1801441.	10.2	105
122	Stable cycling of high-voltage lithium metal batteries in ether electrolytes. Nature Energy, 2018, 3, 739-746.	19.8	767
123	A Localized High-Concentration Electrolyte with Optimized Solvents and Lithium Difluoro(oxalate)borate Additive for Stable Lithium Metal Batteries. ACS Energy Letters, 2018, 3, 2059-2067.	8.8	257
124	Nanovoid Incorporated Ir _{<i>x</i>} Cu Metallic Aerogels for Oxygen Evolution Reaction Catalysis. ACS Energy Letters, 2018, 3, 2038-2044.	8.8	129
125	Electronic response of aluminum-bearing minerals. Journal of Chemical Physics, 2018, 149, 024502.	1.2	11
126	Ultrafine Pd ensembles anchored-Au2Cu aerogels boost ethanol electrooxidation. Nano Energy, 2018, 53, 206-212.	8.2	54

#	Article	IF	CITATIONS
127	Spectroscopic Characterization of Aqua [<i>fac</i> -Tc(CO) ₃] ⁺ Complexes at High Ionic Strength. Inorganic Chemistry, 2018, 57, 6903-6912.	1.9	10
128	Controlled synthesis of highly-branched plasmonic gold nanoparticles through peptoid engineering. Nature Communications, 2018, 9, 2327.	5.8	74
129	Localized High-Concentration Sulfone Electrolytes for High-Efficiency Lithium-Metal Batteries. CheM, 2018, 4, 1877-1892.	5.8	628
130	B4C as a stable non-carbon-based oxygen electrode material for lithium-oxygen batteries. Nano Energy, 2017, 33, 195-204.	8.2	65
131	Probing the Origin of Interfacial Carriers in SrTiO ₃ –LaCrO ₃ Superlattices. Chemistry of Materials, 2017, 29, 1147-1155.	3.2	19
132	Oneâ€Pot Process for Hydrodeoxygenation of Lignin to Alkanes Using Ruâ€Based Bimetallic and Bifunctional Catalysts Supported on Zeolite Y. ChemSusChem, 2017, 10, 1846-1856.	3.6	127
133	Three-dimensional Nitrogen-Doped Reduced Graphene Oxide/Carbon Nanotube Composite Catalysts for Vanadium Flow Batteries. Electroanalysis, 2017, 29, 1469-1473.	1.5	28
134	Revisiting the Corrosion of the Aluminum Current Collector in Lithium-Ion Batteries. Journal of Physical Chemistry Letters, 2017, 8, 1072-1077.	2.1	156
135	Stabilization of Li Metal Anode in DMSOâ€Based Electrolytes via Optimization of Salt–Solvent Coordination for Li–O ₂ Batteries. Advanced Energy Materials, 2017, 7, 1602605.	10.2	99
136	Electrolyte additive enabled fast charging and stable cycling lithium metal batteries. Nature Energy, 2017, 2, .	19.8	1,048
137	Selfâ€Assembled Fe–Nâ€Doped Carbon Nanotube Aerogels with Singleâ€Atom Catalyst Feature as Highâ€Efficiency Oxygen Reduction Electrocatalysts. Small, 2017, 13, 1603407.	5.2	254
138	Formation of Reversible Solid Electrolyte Interface on Graphite Surface from Concentrated Electrolytes. Nano Letters, 2017, 17, 1602-1609.	4.5	91
139	Complete Decomposition of Li ₂ CO ₃ in Li–O ₂ Batteries Using Ir/B ₄ C as Noncarbon-Based Oxygen Electrode. Nano Letters, 2017, 17, 1417-1424.	4.5	104
140	Highly uniform distribution of Pt nanoparticles on N-doped hollow carbon spheres with enhanced durability for oxygen reduction reaction. RSC Advances, 2017, 7, 6303-6308.	1.7	44
141	Tuning the Solid Electrolyte Interphase for Selective Li―and Naâ€ŀon Storage in Hard Carbon. Advanced Materials, 2017, 29, 1606860.	11.1	157
142	Nitrogen and Fluorineâ€Codoped Carbon Nanowire Aerogels as Metalâ€Free Electrocatalysts for Oxygen Reduction Reaction. Chemistry - A European Journal, 2017, 23, 10460-10464.	1.7	52
143	Tetragonal-Like Phase in Core–Shell Iron Iron-Oxide Nanoclusters. Journal of Physical Chemistry C, 2017, 121, 11794-11803.	1.5	3
144	Ambient temperature NO oxidation over Cr-based amorphous mixed oxide catalysts: effects from the second oxide components. Catalysis Science and Technology, 2017, 7, 2362-2370.	2.1	27

#	Article	IF	CITATIONS
145	Template-directed synthesis of nitrogen- and sulfur-codoped carbon nanowire aerogels with enhanced electrocatalytic performance for oxygen reduction. Nano Research, 2017, 10, 1888-1895.	5.8	34
146	Low Pt-content ternary PdCuPt nanodendrites: an efficient electrocatalyst for oxygen reduction reaction. Nanoscale, 2017, 9, 1279-1284.	2.8	66
147	Intermetallic Pd ₃ Pb nanowire networks boost ethanol oxidation and oxygen reduction reactions with significantly improved methanol tolerance. Journal of Materials Chemistry A, 2017, 5, 23952-23959.	5.2	78
148	Temperature Dependence of the Oxygen Reduction Mechanism in Nonaqueous Li–O ₂ Batteries. ACS Energy Letters, 2017, 2, 2525-2530.	8.8	30
149	Revealing the Dynamics of Platinum Nanoparticle Catalysts on Carbon in Oxygen and Water Using Environmental TEM. ACS Catalysis, 2017, 7, 7658-7664.	5.5	38
150	Suppressing Lithium Dendrite Growth by Metallic Coating on a Separator. Advanced Functional Materials, 2017, 27, 1704391.	7.8	141
151	Two-Dimensional N,S-Codoped Carbon/Co ₉ S ₈ Catalysts Derived from Co(OH) ₂ Nanosheets for Oxygen Reduction Reaction. ACS Applied Materials & Interfaces, 2017, 9, 36755-36761.	4.0	45
152	Non-encapsulation approach for high-performance Li–S batteries through controlled nucleation and growth. Nature Energy, 2017, 2, 813-820.	19.8	326
153	Block copolymer templated synthesis of PtIr bimetallic nanocatalysts for the formic acid oxidation reaction. Journal of Materials Chemistry A, 2017, 5, 21514-21527.	5.2	34
154	Toward Rational Design of Cu/SSZ-13 Selective Catalytic Reduction Catalysts: Implications from Atomic-Level Understanding of Hydrothermal Stability. ACS Catalysis, 2017, 7, 8214-8227.	5.5	278
155	Kinetically controlled synthesis of AuPt bi-metallic aerogels and their enhanced electrocatalytic performances. Journal of Materials Chemistry A, 2017, 5, 19626-19631.	5.2	44
156	Suppressed oxygen extraction and degradation of LiNi x Mn y Co z O2 cathodes at high charge cut-off voltages. Nano Research, 2017, 10, 4221-4231.	5.8	77
157	Low-Temperature Pd/Zeolite Passive NO _{<i>x</i>} Adsorbers: Structure, Performance, and Adsorption Chemistry. Journal of Physical Chemistry C, 2017, 121, 15793-15803.	1.5	178
158	Conversion of Methane into Methanol and Ethanol over Nickel Oxide on Ceria–Zirconia Catalysts in a Single Reactor. Angewandte Chemie - International Edition, 2017, 56, 13876-13881.	7.2	44
159	Activation of surface lattice oxygen in single-atom Pt/CeO ₂ for low-temperature CO oxidation. Science, 2017, 358, 1419-1423.	6.0	1,114
160	Sugar Blowingâ€Induced Porous Cobalt Phosphide/Nitrogenâ€Doped Carbon Nanostructures with Enhanced Electrochemical Oxidation Performance toward Water and Other Small Molecules. Small, 2017, 13, 1700796.	5.2	65
161	Reduction and Simultaneous Removal of ⁹⁹ Tc and Cr by Fe(OH) ₂ (s) Mineral Transformation. Environmental Science & Technology, 2017, 51, 8635-8642.	4.6	68
162	Nitrogen–doped graphitized carbon shell encapsulated NiFe nanoparticles: A highly durable oxygen evolution catalyst. Nano Energy, 2017, 39, 245-252.	8.2	143

#	Article	IF	CITATIONS
163	Bimetallic Cobaltâ€Based Phosphide Zeolitic Imidazolate Framework: CoP <i>_x</i> Phaseâ€Dependent Electrical Conductivity and Hydrogen Atom Adsorption Energy for Efficient Overall Water Splitting. Advanced Energy Materials, 2017, 7, 1601555.	10.2	340
164	Electrochemically Controlled Ionâ€exchange Property of Carbon Nanotubes/Polypyrrole Nanocomposite in Various Electrolyte Solutions. Electroanalysis, 2017, 29, 929-936.	1.5	14
165	X-Ray Photoelectron Spectroscopy Applications. , 2017, , 716-724.		15
166	Molecular Storage of Mg Ions with Vanadium Oxide Nanoclusters. Advanced Functional Materials, 2016, 26, 3446-3453.	7.8	65
167	Highly Stable Operation of Lithium Metal Batteries Enabled by the Formation of a Transient Highâ€Concentration Electrolyte Layer. Advanced Energy Materials, 2016, 6, 1502151.	10.2	236
168	Effect of the Anion Activity on the Stability of Li Metal Anodes in Lithium‧ulfur Batteries. Advanced Functional Materials, 2016, 26, 3059-3066.	7.8	117
169	Fabrication of electrocatalytic Ta nanoparticles by reactive sputtering and ion soft landing. Journal of Chemical Physics, 2016, 145, 174701.	1.2	14
170	Kinetically Controlled Synthesis of Pt-Based One-Dimensional Hierarchically Porous Nanostructures with Large Mesopores as Highly Efficient ORR Catalysts. ACS Applied Materials & Interfaces, 2016, 8, 35213-35218.	4.0	53
171	Gallium arsenide (GaAs) (001) after sublimation of arsenic (As) thin-film cap, by XPS. Surface Science Spectra, 2016, 23, 83-92.	0.3	4
172	Gold/silver core-shell 20 nm nanoparticles extracted from citrate solution examined by XPS. Surface Science Spectra, 2016, 23, 29-39.	0.3	6
173	Multimodal and <i>In-Situ</i> Chemical Imaging of Critical Surfaces and Interfaces in Li Batteries. Microscopy Today, 2016, 24, 32-39.	0.2	6
174	Three-dimensional PtNi hollow nanochains as an enhanced electrocatalyst for the oxygen reduction reaction. Journal of Materials Chemistry A, 2016, 4, 8755-8761.	5.2	63
175	Graphene oxide membranes with high permeability and selectivity for dehumidification of air. Carbon, 2016, 106, 164-170.	5.4	54
176	Inorganic tin aluminophosphate nanocomposite for reductive separation of pertechnetate. Environmental Science: Nano, 2016, 3, 1003-1013.	2.2	24
177	The Role of Iron-Bearing Minerals in NO ₂ to HONO Conversion on Soil Surfaces. Environmental Science & Technology, 2016, 50, 8649-8660.	4.6	39
178	Structure and thermodynamic stability of UTa ₃ O ₁₀ , a U(<scp>v</scp>)-bearing compound. Dalton Transactions, 2016, 45, 18892-18899.	1.6	6
179	Enabling room temperature sodium metal batteries. Nano Energy, 2016, 30, 825-830.	8.2	248
180	A Facile Method for Synthesizing Dendritic Core–Shell Structured Ternary Metallic Aerogels and Their Enhanced Electrochemical Performances. Chemistry of Materials, 2016, 28, 7928-7934.	3.2	60

#	Article	IF	CITATIONS
181	Structure and thermodynamics of uranium-containing iron garnets. Geochimica Et Cosmochimica Acta, 2016, 189, 269-281.	1.6	41
182	The importance of solid electrolyte interphase formation for long cycle stability full-cell Na-ion batteries. Nano Energy, 2016, 27, 664-672.	8.2	41
183	PdCuPt Nanocrystals with Multibranches for Enzyme-Free Glucose Detection. ACS Applied Materials & Interfaces, 2016, 8, 22196-22200.	4.0	68
184	Versailles Project on Advanced Materials and Standards Interlaboratory Study on Measuring the Thickness and Chemistry of Nanoparticle Coatings Using XPS and LEIS. Journal of Physical Chemistry C, 2016, 120, 24070-24079.	1.5	33
185	Highly Ordered Mesoporous Bimetallic Phosphides as Efficient Oxygen Evolution Electrocatalysts. ACS Energy Letters, 2016, 1, 792-796.	8.8	139
186	Rational design of efficient electrode–electrolyte interfaces for solid-state energy storage using ion soft landing. Nature Communications, 2016, 7, 11399.	5.8	86
187	Redoxâ€Active Metal–Organic Composites for Highly Selective Oxygen Separation Applications. Advanced Materials, 2016, 28, 3572-3577.	11.1	55
188	Effects of Propylene Carbonate Content in CsPF ₆ -Containing Electrolytes on the Enhanced Performances of Graphite Electrode for Lithium-Ion Batteries. ACS Applied Materials & Interfaces, 2016, 8, 5715-5722.	4.0	43
189	U(<scp>v</scp>) in metal uranates: a combined experimental and theoretical study of MgUO ₄ , CrUO ₄ , and FeUO ₄ . Dalton Transactions, 2016, 45, 4622-4632.	1.6	45
190	Quantifying the Impact of Nanoparticle Coatings and Nonuniformities on XPS Analysis: Gold/Silver Core–Shell Nanoparticles. Analytical Chemistry, 2016, 88, 3917-3925.	3.2	55
191	Hard carbon nanoparticles as high-capacity, high-stability anodic materials for Na-ion batteries. Nano Energy, 2016, 19, 279-288.	8.2	341
192	<mml:math <br="" xmlns:mml="http://www.w3.org/1998/Math/MathML">display="inline"><mml:mrow><mml:msub><mml:mrow><mml:mi>UO</mml:mi></mml:mrow><mml:mn>2Corrosion by Nonclassical Diffusion. Physical Review Letters, 2015, 114, 246103.</mml:mn></mml:msub></mml:mrow></mml:math>	:nanos <td>nlaasub></td>	n laa sub>
193	Inâ€Situâ€Grown ZnCo ₂ O ₄ on Singleâ€Walled Carbon Nanotubes as Air Electrode Materials for Rechargeable Lithium–Oxygen Batteries. ChemSusChem, 2015, 8, 3697-3703.	3.6	34
194	Covalent attachment of diphosphine ligands to glassy carbon electrodes via Cu-catalyzed alkyne-azide cycloaddition. Metallation with Ni(<scp>ii</scp>). Dalton Transactions, 2015, 44, 12225-12233.	1.6	14
195	Dendrite-free Li deposition using trace-amounts of water as an electrolyte additive. Nano Energy, 2015, 15, 135-144.	8.2	297
196	Molecular-confinement of polysulfides within mesoscale electrodes for the practical application of lithium sulfur batteries. Nano Energy, 2015, 13, 267-274.	8.2	50
197	xmlns:mml="http://www.w3.org/1998/Math/MathML" altimg="si1.gif" overflow="scroll"> <mml:mfenced open="(" close=")"><mml:mrow><mml:mn>10</mml:mn><mml:mover accent="true"><mml:mn>1</mml:mn><mml:mo stretchy="true">Â⁻<mml:mn>4</mml:mn></mml:mo </mml:mover </mml:mrow></mml:mfenced 	1.4	18
198	calcite surface. Chemical Geology, 2015, 397, 24-36. Growth and surface modification of LaFeO3 thin films induced by reductive annealing. Applied Surface Science, 2015, 330, 309-315.	3.1	6

#	Article	IF	CITATIONS
199	A Facile Solvothermal Synthesis of Octahedral Fe ₃ O ₄ Nanoparticles. Small, 2015, 11, 2649-2653.	5.2	45
200	Incorporation of Np(V) and U(VI) in carbonate and sulfate minerals crystallized from aqueous solution. Geochimica Et Cosmochimica Acta, 2015, 151, 133-149.	1.6	21
201	New insights into reaction mechanisms of ethanol steam reforming on Co–ZrO2. Applied Catalysis B: Environmental, 2015, 162, 141-148.	10.8	67
202	High rate and stable cycling of lithium metal anode. Nature Communications, 2015, 6, 6362.	5.8	1,954
203	Effect of Co/Ni ratios in cobalt nickel mixed oxide catalysts on methane combustion. Applied Catalysis A: General, 2015, 505, 62-69.	2.2	89
204	Soft landing of bare PtRu nanoparticles for electrochemical reduction of oxygen. Nanoscale, 2015, 7, 12379-12391.	2.8	32
205	Effects of structural defects on the electrochemical activation of Li2MnO3. Nano Energy, 2015, 16, 143-151.	8.2	73
206	An Advanced Na–FeCl ₂ ZEBRA Battery for Stationary Energy Storage Application. Advanced Energy Materials, 2015, 5, 1500357.	10.2	62
207	Charge-Coupled Substituted Garnets (Y _{3–<i>x</i>} Ca _{0.5<i>x</i>} M _{0.5<i>x</i>>/i>})Fe ₅ O _{12(M = Ce, Th): Structure and Stability as Crystalline Nuclear Waste Forms. Inorganic Chemistry, 2015, 54, 4156-4166.}	ub> 1.9	29
208	The Role of Cesium Cation in Controlling Interphasial Chemistry on Graphite Anode in Propylene Carbonate-Rich Electrolytes. ACS Applied Materials & Interfaces, 2015, 7, 20687-20695.	4.0	41
209	Electrical and Magnetic Properties Modification in Heavy Ion Irradiated Nanograin Ni _{<i>x</i>} Co _(3–<i>x</i>) O ₄ Films. Journal of Physical Chemistry C, 2015, 119, 22465-22476.	1.5	14
210	Comparison of 20 nm silver nanoparticles synthesized with and without a gold core: Structure, dissolution in cell culture media, and biological impact on macrophages. Biointerphases, 2015, 10, 031003.	0.6	27
211	Failure Mechanism for Fastâ€Charged Lithium Metal Batteries with Liquid Electrolytes. Advanced Energy Materials, 2015, 5, 1400993.	10.2	540
212	Syntrophic Effects in a Subsurface Clostridial Consortium on Fe(III)-(Oxyhydr)oxide Reduction and Secondary Mineralization. Geomicrobiology Journal, 2014, 31, 101-115.	1.0	13
213	Dendrimerâ€Encapsulated Ruthenium Oxide Nanoparticles as Catalysts in Lithiumâ€Oxygen Batteries. Advanced Functional Materials, 2014, 24, 7510-7519.	7.8	59
214	Dendrite-Free Lithium Deposition with Self-Aligned Nanorod Structure. Nano Letters, 2014, 14, 6889-6896.	4.5	326
215	Investigating commercial cellulase performances toward specific biomass recalcitrance factors using reference substrates. Applied Microbiology and Biotechnology, 2014, 98, 4409-4420.	1.7	19
216	Reduction Mechanism of Fluoroethylene Carbonate for Stable Solid–Electrolyte Interphase Film on Silicon Anode. ChemSusChem, 2014, 7, 549-554.	3.6	126

#	Article	IF	CITATIONS
217	Assigning Oxidation States to Organic Compounds via Predictions from X-ray Photoelectron Spectroscopy: A Discussion of Approaches and Recommended Improvements. Journal of Chemical Education, 2014, 91, 232-238.	1.1	65
218	Effects of Cesium Cations in Lithium Deposition via Self-Healing Electrostatic Shield Mechanism. Journal of Physical Chemistry C, 2014, 118, 4043-4049.	1.5	117
219	Mixed salts of LiTFSI and LiBOB for stable LiFePO4-based batteries at elevated temperatures. Journal of Materials Chemistry A, 2014, 2, 2346.	5.2	85
220	Manipulating surface reactions in lithium–sulphur batteries using hybrid anode structures. Nature Communications, 2014, 5, 3015.	5.8	290
221	Characterization of natural titanomagnetites (Fe3â^'xTixO4) for studying heterogeneous electron transfer to Tc(VII) in the Hanford subsurface. Geochimica Et Cosmochimica Acta, 2014, 128, 114-127.	1.6	20
222	Electrodeposition from Acidic Solutions of Nickel Bis(benzenedithiolate) Produces a Hydrogen-Evolving Ni–S Film on Glassy Carbon. ACS Catalysis, 2014, 4, 90-98.	5.5	59
223	Controlling SEI Formation on SnSbâ€Porous Carbon Nanofibers for Improved Na Ion Storage. Advanced Materials, 2014, 26, 2901-2908.	11.1	441
224	The role of FeS in initial activation and performance degradation of Na–NiCl2 batteries. Journal of Power Sources, 2014, 272, 398-403.	4.0	29
225	Formation of Interfacial Layer and Long-Term Cyclability of Li–O ₂ Batteries. ACS Applied Materials & Interfaces, 2014, 6, 14141-14151.	4.0	44
226	Synergistic Catalysis between Pd and Fe in Gas Phase Hydrodeoxygenation of <i>m</i> -Cresol. ACS Catalysis, 2014, 4, 3335-3345.	5.5	173
227	Oxidative Remobilization of Technetium Sequestered by Sulfide-Transformed Nano Zerovalent Iron. Environmental Science & Technology, 2014, 48, 7409-7417.	4.6	73
228	The Mechanisms of Oxygen Reduction and Evolution Reactions in Nonaqueous Lithium–Oxygen Batteries. ChemSusChem, 2014, 7, 2436-2440.	3.6	62
229	A General Mechanism for Stabilizing the Small Sizes of Precious Metal Nanoparticles on Oxide Supports. Chemistry of Materials, 2014, 26, 5475-5481.	3.2	53
230	Lewis Acid–Base Interactions between Polysulfides and Metal Organic Framework in Lithium Sulfur Batteries. Nano Letters, 2014, 14, 2345-2352.	4.5	623
231	Impact of a Mixed Oxide's Surface Composition and Structure on Its Adsorptive Properties: Case of the (Fe,Cr) ₃ O ₄ (111) Termination of the α-(Fe,Cr) ₂ O ₃ (0001) Surface. Journal of Physical Chemistry C, 2014, 118, 29058-29067.	1.5	11
232	Surface Plasmon-Driven Water Reduction: Gold Nanoparticle Size Matters. Journal of the American Chemical Society, 2014, 136, 9842-9845.	6.6	301
233	Electrochemically stable cathode current collectors for rechargeable magnesium batteries. Journal of Materials Chemistry A, 2014, 2, 2473-2477.	5.2	77
234	Microstructure and Cs Behavior of Ba-Doped Aluminosilicate Pollucite Irradiated with F ⁺ Ions. Journal of Physical Chemistry C, 2014, 118, 18160-18169.	1.5	7

#	Article	IF	CITATIONS
235	Atomic-Structural Synergy for Catalytic CO Oxidation over Palladium–Nickel Nanoalloys. Journal of the American Chemical Society, 2014, 136, 7140-7151.	6.6	104
236	A Hydrogen-Evolving Ni(P ₂ N ₂) ₂ Electrocatalyst Covalently Attached to a Glassy Carbon Electrode: Preparation, Characterization, and Catalysis. Comparisons with the Homogeneous Analogue. Inorganic Chemistry, 2014, 53, 6875-6885.	1.9	49
237	Direct Observation of Li2O2 Nucleation and Growth with In-Situ Liquid ec-(S)TEM. Microscopy and Microanalysis, 2014, 20, 1608-1609.	0.2	Ο
238	Reductive Sequestration of Pertechnetate (⁹⁹ TcO ₄ [–]) by Nano Zerovalent Iron (nZVI) Transformed by Abiotic Sulfide. Environmental Science & Technology, 2013, 47, 5302-5310.	4.6	162
239	Surface-Driven Sodium Ion Energy Storage in Nanocellular Carbon Foams. Nano Letters, 2013, 13, 3909-3914.	4.5	245
240	Minimal Proton Channel Enables H ₂ Oxidation and Production with a Water-Soluble Nickel-Based Catalyst. Journal of the American Chemical Society, 2013, 135, 18490-18496.	6.6	131
241	Electrocatalytic properties of poly(3,4-ethylenedioxythiophene) (PEDOT) in Li-O2 battery. Electrochemistry Communications, 2013, 29, 63-66.	2.3	36
242	The Electrode as Organolithium Reagent: Catalyst-Free Covalent Attachment of Electrochemically Active Species to an Azide-Terminated Glassy Carbon Electrode Surface. Inorganic Chemistry, 2013, 52, 13674-13684.	1.9	10
243	Bifunctional nanoparticles for SERS monitoring and magnetic intervention of assembly and enzyme cutting of DNAs. Journal of Materials Chemistry B, 2013, 1, 4320.	2.9	27
244	Al2O3 e-Beam Evaporated onto Silicon (100)/SiO2, by XPS. Surface Science Spectra, 2013, 20, 43-48.	0.3	29
245	Surface characterization of nanomaterials and nanoparticles: Important needs and challenging opportunities. Journal of Vacuum Science and Technology A: Vacuum, Surfaces and Films, 2013, 31, 50820.	0.9	227
246	Thermally Annealed Iron (Oxide) Thin Film on an Alumina Barrier Layer, by XPS. Surface Science Spectra, 2013, 20, 55-61.	0.3	11
247	Watermelon-like iron nanoparticles: Cr doping effect on magnetism and magnetization interaction reversal. Nanoscale, 2013, 5, 7872.	2.8	17
248	Very Stable Electron Field Emission from Strontium Titanate Coated Carbon Nanotube Matrices with Low Emission Thresholds. ACS Nano, 2013, 7, 117-125.	7.3	60
249	Continuous precipitation of ceria nanoparticles from a continuous flow micromixer. International Journal of Advanced Manufacturing Technology, 2013, 64, 579-586.	1.5	17
250	Stability of polymer binders in Li–O 2 batteries. Journal of Power Sources, 2013, 243, 899-907.	4.0	102
251	An advanced understanding of the specific effects of xylan and surface lignin contents on enzymatic hydrolysis of lignocellulosic biomass. Bioresource Technology, 2013, 132, 137-145.	4.8	115
252	Effects of Electrolyte Salts on the Performance of Li–O ₂ Batteries. Journal of Physical Chemistry C, 2013, 117, 2635-2645.	1.5	204

#	Article	IF	CITATIONS
253	Dendrite-Free Lithium Deposition via Self-Healing Electrostatic Shield Mechanism. Journal of the American Chemical Society, 2013, 135, 4450-4456.	6.6	1,736
254	Surface Plasmon Mediated Chemical Solution Deposition of Gold Nanoparticles on a Nanostructured Silver Surface at Room Temperature. Journal of the American Chemical Society, 2013, 135, 38-41.	6.6	60
255	Molecular structures of polymer/sulfur composites for lithium–sulfur batteries with long cycle life. Journal of Materials Chemistry A, 2013, 1, 9517.	5.2	59
256	Ionic liquid-enhanced solid state electrolyte interface (SEI) for lithium–sulfur batteries. Journal of Materials Chemistry A, 2013, 1, 8464.	5.2	229
257	Silicon (100)/SiO2 by XPS. Surface Science Spectra, 2013, 20, 36-42.	0.3	134
258	Multiwalled Carbon Nanotube Forest Grown via Chemical Vapor Deposition from Iron Catalyst Nanoparticles, by XPS. Surface Science Spectra, 2013, 20, 62-67.	0.3	19
259	Coordination Chemistry in magnesium battery electrolytes: how ligands affect their performance. Scientific Reports, 2013, 3, 3130.	1.6	157
260	Effects of Carbonate Solvents and Lithium Salts on Morphology and Coulombic Efficiency of Lithium Electrode. Journal of the Electrochemical Society, 2013, 160, A1894-A1901.	1.3	260
261	Thermally Evaporated Iron (Oxide) on an Alumina Barrier Layer, by XPS. Surface Science Spectra, 2013, 20, 49-54.	0.3	14
262	Multiâ€instrument characterization of the surfaces and materials in microfabricated, carbon nanotubeâ€templated thin layer chromatography plates. An analogy to â€~The Blind Men and the Elephant'. Surface and Interface Analysis, 2013, 45, 1273-1282.	0.8	52
263	Magnetic interaction reversal in watermelon nanostructured Cr-doped Fe nanoclusters. Applied Physics Letters, 2013, 103, .	1.5	6
264	Study of surface cleaning methods and pyrolysis temperatures on nanostructured carbon films using x-ray photoelectron spectroscopy. Journal of Vacuum Science and Technology A: Vacuum, Surfaces and Films, 2012, 30, 061407.	0.9	7
265	Stable, microfabricated thin layer chromatography plates without volume distortion on patterned, carbon and Al2O3-primed carbon nanotube forests. Journal of Chromatography A, 2012, 1257, 195-203.	1.8	42
266	Effect of sulfur loading on the desulfation chemistry of a commercial lean NOx trap catalyst. Catalysis Today, 2012, 197, 3-8.	2.2	11
267	Gold–Copper Nanoparticles: Nanostructural Evolution and Bifunctional Catalytic Sites. Chemistry of Materials, 2012, 24, 4662-4674.	3.2	85
268	Inhibition of Trace Element Release During Fe(II)-Activated Recrystallization of Al-, Cr-, and Sn-Substituted Goethite and Hematite. Environmental Science & Technology, 2012, 46, 10031-10039.	4.6	61
269	Role of Support–Nanoalloy Interactions in the Atomic-Scale Structural and Chemical Ordering for Tuning Catalytic Sites. Journal of the American Chemical Society, 2012, 134, 15048-15060.	6.6	89
270	Comparative Study on the Sulfur Tolerance and Carbon Resistance of Supported Noble Metal Catalysts in Steam Reforming of Liquid Hydrocarbon Fuel. ACS Catalysis, 2012, 2, 1127-1137.	5.5	63

#	Article	IF	CITATIONS
271	Physical properties and surface/interface analysis of nanocrystalline WO3 films grown under variable oxygen gas flow rates. Applied Surface Science, 2012, 259, 172-177.	3.1	8
272	Performance of solid oxide fuel cells operated with coal syngas provided directly from a gasification process. Journal of Power Sources, 2012, 214, 142-152.	4.0	29
273	The stability of organic solvents and carbon electrode in nonaqueous Li-O2 batteries. Journal of Power Sources, 2012, 215, 240-247.	4.0	197
274	Correlation between Surface Chemistry, Density, and Band Gap in Nanocrystalline WO ₃ Thin Films. ACS Applied Materials & Interfaces, 2012, 4, 1371-1377.	4.0	135
275	Influence of Aging and Environment on Nanoparticle Chemistry: Implication to Confinement Effects in Nanoceria. Journal of Physical Chemistry C, 2012, 116, 14108-14114.	1.5	103
276	Reduction of U(VI) Incorporated in the Structure of Hematite. Environmental Science & Technology, 2012, 46, 9428-9436.	4.6	82
277	An investigation of hydrogen depth profiling using ToFâ€SIMS. Surface and Interface Analysis, 2012, 44, 232-237.	0.8	33
278	Effects of cell positive cans and separators on the performance of high-voltage Li-ion batteries. Journal of Power Sources, 2012, 213, 160-168.	4.0	44
279	Role of Metal Coordination Structures in Enhancement of Electrocatalytic Activity of Ternary Nanoalloys for Oxygen Reduction Reaction. ACS Catalysis, 2012, 2, 795-806.	5.5	62
280	Hollow core–shell structured porous Si–C nanocomposites for Li-ion battery anodes. Journal of Materials Chemistry, 2012, 22, 11014.	6.7	280
281	Enhanced performance of graphite anode materials by AlF3 coating for lithium-ion batteries. Journal of Materials Chemistry, 2012, 22, 12745.	6.7	129
282	Correlation of Pt–Re surface properties with reaction pathways for the aqueous-phase reforming of glycerol. Journal of Catalysis, 2012, 287, 37-43.	3.1	118
283	A Soft Approach to Encapsulate Sulfur: Polyaniline Nanotubes for Lithiumâ€5ulfur Batteries with Long Cycle Life. Advanced Materials, 2012, 24, 1176-1181.	11.1	959
284	Catalytic Roles of Co ^O and Co ²⁺ during Steam Reforming of Ethanol on Co/MgO Catalysts. ACS Catalysis, 2011, 1, 279-286.	5.5	98
285	display="inline"> <mml:msub><mml:mrow /><mml:mrow><mml:mn>3</mml:mn><mml:mo>â^'</mml:mo><mml:mi>x</mml:mi></mml:mrow></mml:mrow </mml:msub> xmlns:mml="http://www.w3.org/1998/Math/MathML" display="inline"> <mml:msub><mml:mrow /><mml:mi>x</mml:mi></mml:mrow </mml:msub> O <mml:math< td=""><td>1.1</td><td>ath>Ti<mm 15</mm </td></mml:math<>	1.1	ath>Ti <mm 15</mm
286	zinins:mml="http://www.w3.org/1998/Math/Math/Math/M2" display="inline"> <mmlansub><mmlanrow // amount The role of H2O in the carbonation of forsterite in supercritical CO2. International Journal of Greenhouse Gas Control, 2011, 5, 1081-1092.</mmlanrow </mmlansub>	2.3	103
287	Functionalized Graphene Oxide as a Nanocarrier in a Multienzyme Labeling Amplification Strategy for Ultrasensitive Electrochemical Immunoassay of Phosphorylated p53 (S392). Analytical Chemistry, 2011, 83, 746-752.	3.2	305
288	Thickness Dependency of Thin-Film Samaria-Doped Ceria for Oxygen Sensing. IEEE Sensors Journal, 2011, 11, 217-224.	2.4	14

#	Article	IF	CITATIONS
289	Polyelectrolyte-Induced Reduction of Exfoliated Graphite Oxide: A Facile Route to Synthesis of Soluble Graphene Nanosheets. ACS Nano, 2011, 5, 1785-1791.	7.3	293
290	Heterogeneous reduction of U6+ by structural Fe2+ from theory and experiment. Geochimica Et Cosmochimica Acta, 2011, 75, 7277-7290.	1.6	64
291	Self assembly of acetylcholinesterase on a gold nanoparticles–graphene nanosheet hybrid for organophosphate pesticide detection using polyelectrolyte as a linker. Journal of Materials Chemistry, 2011, 21, 5319.	6.7	219
292	Ultrafine Particulate Ferrous Iron and Anthracene Associations with Mitochondrial Dysfunction. Aerosol Science and Technology, 2011, 45, 1109-1122.	1.5	18
293	Nitrogen-incorporation induced changes in the microstructure of nanocrystalline WO3 thin films. Thin Solid Films, 2011, 520, 1446-1450.	0.8	18
294	Correlation between Atomic Coordination Structure and Enhanced Electrocatalytic Activity for Trimetallic Alloy Catalysts. Journal of the American Chemical Society, 2011, 133, 12714-12727.	6.6	96
295	The Effect of Zinc Addition on the Oxidation State of Cobalt in Co/ZrO ₂ Catalysts. ChemSusChem, 2011, 4, 1679-1684.	3.6	36
296	Growth, microstructure and electrical properties of sputter-deposited hafnium oxide (HfO2) thin films grown using a HfO2 ceramic target. Applied Surface Science, 2011, 257, 2197-2202.	3.1	39
297	Effects of tungsten oxide addition on the electrochemical performance of nanoscale tantalum oxide-based electrocatalysts for proton exchange membrane (PEM) fuel cells. Journal of Power Sources, 2011, 196, 6099-6103.	4.0	27
298	Beam damage of HS(CH2)15 COOH Terminated Self Assembled Monolayer (SAM) as Observed by X-ray Photoelectron Spectroscopy. Surface Science Spectra, 2011, 18, 68-81.	0.3	1
299	As-Received,Ozone Cleaned and Ar+ Sputtered Surfaces of Hafnium Oxide Grown by Atomic Layer Deposition and Studied by XPS. Surface Science Spectra, 2011, 18, 46-57.	0.3	20
300	Mitigation of Sulfur Poisoning of Ni/Zirconia SOFC Anodes by Antimony and Tin. Journal of the Electrochemical Society, 2011, 158, B424.	1.3	31
301	Enhanced Electron Field Emission from Carbon Nanotube Matrices. Materials Research Society Symposia Proceedings, 2011, 1283, 1.	0.1	0
302	Microstructure of the Native Oxide Layer on Ni and Cr-Doped Ni Nanoparticles. Journal of Nanoscience and Nanotechnology, 2011, 11, 8488-8497.	0.9	21
303	The Importance of Complementary Information Provided by Surface Analysis, Electron Microscopy and in situ Characterization of Nanoparticles. Microscopy and Microanalysis, 2010, 16, 408-409.	0.2	1
304	Compositional tuning of ultrathin surface oxides on metal and alloy substrates using photons: Dynamic simulations and experiments. Physical Review B, 2010, 81, .	1.1	13
305	Nitrogen-doped graphene and its electrochemical applications. Journal of Materials Chemistry, 2010, 20, 7491.	6.7	1,040
306	Microbial and Mineralogical Characterizations of Soils Collected from the Deep Biosphere of the Former Homestake Gold Mine, South Dakota. Microbial Ecology, 2010, 60, 539-550.	1.4	70

#	Article	IF	CITATIONS
307	Nitrogen-doped mesoporous carbon for energy storage in vanadium redox flow batteries. Journal of Power Sources, 2010, 195, 4375-4379.	4.0	306
308	Stabilization of ZnMnO3 phase from sol–gel synthesized nitrate precursors. Journal of Sol-Gel Science and Technology, 2010, 53, 141-147.	1.1	30
309	Ethanol synthesis from syngas over Rh-based/SiO2 catalysts: A combined experimental and theoretical modeling study. Journal of Catalysis, 2010, 271, 325-342.	3.1	174
310	Water-induced formation of cobalt oxides over supported cobalt/ceria–zirconia catalysts under ethanol-steam conditions. Journal of Catalysis, 2010, 273, 229-235.	3.1	77
311	Highâ€Performance, Superparamagnetic, Nanoparticleâ€Based Heavy Metal Sorbents for Removal of Contaminants from Natural Waters. ChemSusChem, 2010, 3, 749-757.	3.6	117
312	Photochemical Reactions of Poly(4â€vinylphenol) Thin Films. Macromolecular Chemistry and Physics, 2010, 211, 461-470.	1.1	11
313	XPS analysis of nanostructured materials and biological surfaces. Journal of Electron Spectroscopy and Related Phenomena, 2010, 178-179, 415-432. Instability, intermixing and electronic structure at the epitaxial (mml:math	0.8	177
314	Instability, intermixing and electronic structure at the epitaxial <mml:math xmlns:mml="http://www.w3.org/1998/Math/MathML" altimg="si51.gif" display="inline" overflow="scroll"> <mml:msub> <mml:mrow> <mml:mstyle mathvariant="normal"> <mml:mi> LaAlO </mml:mi> </mml:mstyle </mml:mrow> <mml:mrow> <mml:mn> 3 <td>nn><td>:mrow></td></td></mml:mn></mml:mrow></mml:msub></mml:math 	nn> <td>:mrow></td>	:mrow>

#	Article	IF	CITATIONS
325	Facile and controllable electrochemical reduction of graphene oxide and its applications. Journal of Materials Chemistry, 2010, 20, 743-748.	6.7	787
326	Mechanistic Studies on Room Temperature Photoexcitation Effects on Passivity Breakdown of Ultrathin Surface Oxide Films Formed on Ternary Alâ^'5%Cuâ^'5%Ni Alloys. Journal of Physical Chemistry C, 2010, 114, 17788-17795.	1.5	1
327	Nanoscale Alloying, Phase-Segregation, and Coreâ^'Shell Evolution of Goldâ ''Platinum Nanoparticles and Their Electrocatalytic Effect on Oxygen Reduction Reaction. Chemistry of Materials, 2010, 22, 4282-4294.	3.2	205
328	Role of extracellular polymeric substances in bioflocculation of activated sludge microorganisms under glucose-controlled conditions. Water Research, 2010, 44, 4505-4516.	5.3	396
329	Comparison of the sputter rates of oxide films relative to the sputter rate of SiO2. Journal of Vacuum Science and Technology A: Vacuum, Surfaces and Films, 2010, 28, 1060-1072.	0.9	122
330	Nonstoichiometric material transfer in the pulsed laser deposition of LaAlO3. Applied Physics Letters, 2010, 97, .	1.5	43
331	Chromium-assisted synthesis of platinum nanocube electrocatalysts. Chemical Communications, 2010, 46, 7184.	2.2	46
332	Suppression of conductivity in Mn-doped ZnO thin films. Journal of Applied Physics, 2009, 105, .	1.1	42
333	Growth-rate induced epitaxial orientation of CeO2 on Al2O3(0001). Applied Physics Letters, 2009, 94, 204101.	1.5	14
334	New Approaches for Characterizing Sensor and Other Modern Complex Materials. ECS Transactions, 2009, 19, 137-148.	0.3	0
335	Performance Evaluation of an Oxygen Sensor as a Function of the Samaria Doped Ceria Film Thickness. Materials Research Society Symposia Proceedings, 2009, 1209, 1.	0.1	1
336	Microstructure and secondary phase segregation correlation in epitaxial/oriented ZnO films with unfavorable Cr dopant. Journal of Materials Research, 2009, 24, 506-515.	1.2	3
337	Changes in the quaternary structure of amelogenin when adsorbed onto surfaces. Biopolymers, 2009, 91, 103-107.	1.2	41
338	Raman and XPS characterization of fuel–cladding interactions using miniature specimens. Journal of Nuclear Materials, 2009, 383, 237-243.	1.3	5
339	Long-term black carbon dynamics in cultivated soil. Biogeochemistry, 2009, 92, 163-176.	1.7	133
340	Promotional Effect of CO2 on Desulfation Processes for Pre-Sulfated Pt-BaO/Al2O3 Lean NOx Trap Catalysts. Topics in Catalysis, 2009, 52, 1719-1722.	1.3	3
341	Fluorescent dye encapsulated ZnO particles with cell-specific toxicity for potential use in biomedical applications. Journal of Materials Science: Materials in Medicine, 2009, 20, 11-22.	1.7	121
342	Enhanced activity and stability of Pt catalysts on functionalized graphene sheets for electrocatalytic oxygen reduction. Electrochemistry Communications, 2009, 11, 954-957.	2.3	615

#	Article	IF	CITATIONS
343	The corrosion of PEM fuel cell catalyst supports and its implications for developing durable catalysts. Electrochimica Acta, 2009, 54, 3109-3114.	2.6	100
344	Influence of samaria doping on the resistance of ceria thin films and its implications to the planar oxygen sensing devices. Sensors and Actuators B: Chemical, 2009, 139, 380-386.	4.0	26
345	Accelerated testing of HT-9 with zirconia coatings containing gallium using Raman Spectroscopy and XPS. Journal of Nuclear Materials, 2009, 395, 23-29.	1.3	2
346	Electrochemical investigation of polyhalide ion oxidation–reduction on carbon nanotube electrodes for redox flow batteries. Electrochemistry Communications, 2009, 11, 2064-2067.	2.3	36
347	Effects of Sulfation Level on the Desulfation Behavior of Presulfated Pt-BaO/Al ₂ O ₃ Lean NO <i>_x</i> Trap Catalysts: A Combined H ₂ Temperature-Programmed Reaction, in Situ Sulfur K-Edge X-ray Absorption Near-Edge Spectroscopy, X-ray Photoelectron Spectroscopy, and Time-Resolved X-ray Diffraction Study. Journal	1.5	17
348	Adsorption of Amelogenin onto Self-Assembled and Fluoroapatite Surfaces. Journal of Physical Chemistry B, 2009, 113, 1833-1842.	1.2	48
349	Growth and Characterization of Barium Oxide Nanoclusters on YSZ(111). Journal of Physical Chemistry C, 2009, 113, 14324-14328.	1.5	15
350	Interparticle Chiral Recognition of Enantiomers: A Nanoparticle-Based Regulation Strategy. Analytical Chemistry, 2009, 81, 689-698.	3.2	82
351	On the Relationship between Nonstoichiometry and Passivity Breakdown in Ultrathin Oxides: Combined Depth-Dependent Spectroscopy, Mottâ^Schottky Analysis, and Molecular Dynamics Simulation Studies. Journal of Physical Chemistry C, 2009, 113, 3502-3511.	1.5	30
352	Defining Active Catalyst Structure and Reaction Pathways from ab Initio Molecular Dynamics and Operando XAFS: Dehydrogenation of Dimethylaminoborane by Rhodium Clusters. Journal of the American Chemical Society, 2009, 131, 10516-10524.	6.6	67
353	Using Thin Films to Screen Possible Scintillator Materials. IEEE Transactions on Nuclear Science, 2009, 56, 1650-1654.	1.2	2
354	Morphology and Electronic Structure of the Oxide Shell on the Surface of Iron Nanoparticles. Journal of the American Chemical Society, 2009, 131, 8824-8832.	6.6	218
355	Fine Structural Features and Electronic Structure of Core-Shell Structured Fe Nanoparticles Probed using TEM/STEM and EELS. Microscopy and Microanalysis, 2009, 15, 1204-1205.	0.2	4
356	Effect of Coal Gas Contaminants on Solid Oxide Fuel Cell Operation. ECS Transactions, 2008, 11, 63-70.	0.3	7
357	Long-term black carbon dynamics in cultivated soil. Biogeochemistry, 2008, 89, 295-308.	1.7	186
358	Electrodeposition of technetium on platinum for thermal ionization mass spectrometry (TIMS). Journal of Radioanalytical and Nuclear Chemistry, 2008, 276, 493-498.	0.7	4
359	Characterization challenges for nanomaterials. Surface and Interface Analysis, 2008, 40, 529-537.	0.8	121
360	Growth and structure of epitaxial Ce0.8Sm0.2O1.9 by oxygen-plasma-assisted molecular beam epitaxy. Journal of Crystal Growth, 2008, 310, 2450-2456.	0.7	21

#	Article	IF	CITATIONS
361	Effect of nitrogen additives on flame retardant action of tributyl phosphate: Phosphorus–nitrogen synergism. Polymer Degradation and Stability, 2008, 93, 99-108.	2.7	213
362	The synthesis of Ag-doped mesoporous TiO2. Microporous and Mesoporous Materials, 2008, 111, 639-642.	2.2	29
363	Controlling size of gold clusters in polyaniline from top–down and from bottom–up. Journal of Electroanalytical Chemistry, 2008, 621, 238-244.	1.9	26
364	N incorporation, composition and electronic structure in N-doped TiO2(001) anatase epitaxial films grown on LaAlO3(001). Surface Science, 2008, 602, 133-141.	0.8	38
365	Growth and characterization of highly oriented gadolinia-doped ceria (111) thin films on zirconia (111)/sapphire (0001) substrates. Thin Solid Films, 2008, 516, 6088-6094.	0.8	15
366	Effects of atmospheres on bonding characteristics of silver and alumina. International Journal of Hydrogen Energy, 2008, 33, 4001-4011.	3.8	11
367	Low-Temperature Synthesis of Tunable Mesoporous Crystalline Transition Metal Oxides and Applications as Au Catalyst Supports. Journal of Physical Chemistry C, 2008, 112, 13499-13509.	1.5	81
368	Characterization of CeO2-supported Cu–Pd bimetallic catalyst for the oxygen-assisted water–gas shift reaction. Journal of Catalysis, 2008, 260, 358-370.	3.1	138
369	Superior nanoscale passive oxide layers synthesized under photon irradiation for environmental protection. Applied Physics Letters, 2008, 92, 263103.	1.5	15
370	Spectroscopic Characterization of Extracellular Polymeric Substances from <i>Escherichia coli</i> and <i>Serratia marcescens</i> : Suppression Using Sub-Inhibitory Concentrations of Bismuth Thiols. Biomacromolecules, 2008, 9, 3079-3089.	2.6	113
371	Role of dopant incorporation on the magnetic properties of Ce1â^'xNixO2 nanoparticles: An electron paramagnetic resonance study. Journal of Applied Physics, 2008, 103, .	1.1	22
372	Natural oxidation of black carbon in soils: Changes in molecular form and surface charge along a climosequence. Geochimica Et Cosmochimica Acta, 2008, 72, 1598-1610.	1.6	733
373	Stability of biomass-derived black carbon in soils. Geochimica Et Cosmochimica Acta, 2008, 72, 6069-6078.	1.6	287
374	Synthesis of lutetium phosphate–apoferritin core–shell nanoparticles for potential applications in radioimmunoimaging and radioimmunotherapy of cancers. Journal of Materials Chemistry, 2008, 18, 1779.	6.7	44
375	Surface and Interface Properties of 10–12 Unit Cells Thick Sputter Deposited Epitaxial CeO ₂ Films. Research Letters in Materials Science, 2008, 2008, 1-5.	0.2	0
376	Conductivity of Oriented Samaria-Doped Ceria Thin Films Grown by Oxygen-Plasma-Assisted Molecular Beam Epitaxy. Electrochemical and Solid-State Letters, 2008, 11, B76.	2.2	13
377	Direct measurement of oxygen incorporation into thin film oxides at room temperature upon ultraviolet photon irradiation. Applied Physics Letters, 2008, 93, .	1.5	5
378	Hidden ferromagnetic secondary phases in cobalt-doped ZnO epitaxial thin films. Physical Review B, 2008, 77, .	1.1	168

#	Article	IF	CITATIONS
379	Variation of Oxygen-to-Carbon Ratio in Oxyacetylene Flame. , 2008, , .		1
380	Inhibition of mitochondrial electron transport by atmospheric ultrafine particles: ferrous iron, quinones and ROS production. FASEB Journal, 2008, 22, 264-264.	0.2	0
381	Metalorganic chemical vapor deposition of carbon-free ZnO using the bis(2,2,6,6-tetramethyl-3,5-heptanedionato)zinc precursor. Journal of Materials Research, 2007, 22, 1230-1234.	1.2	14
382	Nucleation and Growth of MOCVD Grown (Cr, Zn)O Films. Journal of the Electrochemical Society, 2007, 154, D134.	1.3	6
383	Ferromagnetic semiconductor nanoclusters: Co-doped Cu2O. Applied Physics Letters, 2007, 90, 013106.	1.5	20
384	Morphology and oxide shell structure of iron nanoparticles grown by sputter-gas-aggregation. Nanotechnology, 2007, 18, 255603.	1.3	59
385	Behavior of Si and C atoms in ion amorphized SiC. Journal of Applied Physics, 2007, 101, 023524.	1.1	26
386	Novel magnetic hydrogen sensing: a case study using antiferromagnetic haematite nanoparticles. Nanotechnology, 2007, 18, 165502.	1.3	30
387	Ferromagnetism in chemically synthesized <mml:math xmlns:mml="http://www.w3.org/1998/Math/MathML" display="inline"> <mml:mrow> <mml:mi mathvariant="normal">Ce <mml:msub> <mml:mi mathvariant="normal">Ce <mml:mn>2 </mml:mn></mml:mi </mml:msub> </mml:mi </mml:mrow> nanopartic</mml:math 	1.1 les	156
388	by Widoping. Physical Review 8, 2007, 76, . Electrochemical effects of S accumulation on ion-implanted Alloy 22 in 1M NaCl solutions. Corrosion Science, 2007, 49, 2497-2511.	3.0	2
389	On the room-temperature ferromagnetism of Zn1â^'xCrxO thin films deposited by reactive co-sputtering. Solar Energy Materials and Solar Cells, 2007, 91, 1496-1502.	3.0	19
390	Epitaxial growth and microstructure of Cu2O nanoparticle/thin films on SrTiO3(100). Nanotechnology, 2007, 18, 115601.	1.3	42
391	Effect of Co doping on the structural, optical and magnetic properties of ZnO nanoparticles. Journal of Physics Condensed Matter, 2007, 19, 266203.	0.7	88
392	N incorporation and electronic structure in N-doped TiO2(110) rutile. Surface Science, 2007, 601, 1754-1762.	0.8	79
393	Electron beam-induced thickening of the protective oxide layer around Fe nanoparticles. Ultramicroscopy, 2007, 108, 43-51.	0.8	53
394	Synthesis and characterization of phosphate-coated mesoporous titania and Cd-doping of same via ion-exchange. Inorganic Chemistry Communication, 2007, 10, 642-645.	1.8	12
395	The synthesis of cadmium doped mesoporous TiO2. Inorganic Chemistry Communication, 2007, 10, 639-641.	1.8	19
396	Functional mesoporous carbon built from the 1,10-phenanthroline building block: A new class of catalyst support. Inorganic Chemistry Communication, 2007, 10, 1541-1544.	1.8	7

#	Article	IF	CITATIONS
397	Synthesis and characterization of compositionally graded Si1â^'xGex layers on Si substrate. Nuclear Instruments & Methods in Physics Research B, 2007, 261, 723-726.	0.6	1
398	Fabrication of SiO2 microdisk arrays for optics and light trapping experiments. Microelectronic Engineering, 2007, 84, 2799-2803.	1.1	1
399	Effect of Mn doping on the structural, morphological, optical and magnetic properties of indium tin oxide films. Journal of Materials Science: Materials in Electronics, 2007, 18, 1197-1201.	1.1	23
400	Degradation Mechanisms of La–Sr–Co–Fe–O[sub 3] SOFC Cathodes. Electrochemical and Solid-State Letters, 2006, 9, A478.	2.2	329
401	Development and processing temperature dependence of ferromagnetism in Zn0.98Co0.02O. Journal of Applied Physics, 2006, 99, 08M123.	1.1	31
402	Sensitive Immunoassay of a Biomarker Tumor Necrosis Factor-α Based on Poly(guanine)-Functionalized Silica Nanoparticle Label. Analytical Chemistry, 2006, 78, 6974-6979.	3.2	172
403	Magnetic gas sensing using a dilute magnetic semiconductor. Applied Physics Letters, 2006, 89, 112509.	1.5	64
404	Ferromagnetism in Ti-Doped ZnO Nanoclusters above Room Temperature. , 2006, , .		0
405	Surface and Interface Control on Photochemically Initiated Immobilization. Journal of the American Chemical Society, 2006, 128, 14067-14072.	6.6	47
406	Oxidation of black carbon by biotic and abiotic processes. Organic Geochemistry, 2006, 37, 1477-1488.	0.9	942
407	In-Situ Growth of Passivation Oxide Layer on Fe-Nanoparticle under Electron-Beam Irradiation in a TEM. Microscopy and Microanalysis, 2006, 12, 546-547.	0.2	0
408	Synthesis of room-temperature ferromagnetic Cr-doped TiO2(1 1 0) rutile single crystals using ion implantation. Nuclear Instruments & Methods in Physics Research B, 2006, 242, 198-200.	0.6	17
409	Dopant distribution, oxygen stoichiometry and magnetism of nanoscale Sn0.99Co0.01O2. Solid State Communications, 2006, 139, 434-438.	0.9	19
410	Distribution of oxygen vacancies and gadolinium dopants in ZrO2–CeO2 multi-layer films grown on α-Al2O3. Solid State Ionics, 2006, 177, 1299-1306.	1.3	15
411	Effects of nanocrystalline CeO2 supports on the properties and performance of Ni–Rh bimetallic catalyst for oxidative steam reforming of ethanol. Journal of Catalysis, 2006, 238, 430-440.	3.1	252
412	Ferromagnetism in Ti-Doped ZnO Nanoclusters Above Room Temperature. IEEE Transactions on Magnetics, 2006, 42, 2697-2699.	1.2	21
413	Preparation, Characterization and Anion Exchange Properties of Polypyrrole/Carbon Nanotube Nanocomposites. Journal of Nanoscience and Nanotechnology, 2006, 6, 547-553.	0.9	18
414	Correlation among Channeling, Morphological, and Microstructural Properties in Epitaxial CeO[sub 2] Films. Electrochemical and Solid-State Letters, 2006, 9, J17.	2.2	4

#	Article	IF	CITATIONS
415	Chemical bonding and electronic structures of the Al2SiO5 polymorphs, andalusite, sillimanite, and kyanite: X-ray photoelectron- and electron energy loss spectroscopy studies. American Mineralogist, 2006, 91, 740-746.	0.9	29
416	Characterization of Microstructure and Composition of Fe-B Nanobars as Biosensor Platform. Materials Research Society Symposia Proceedings, 2006, 962, 1.	0.1	2
417	Irradiation behavior of SrTiO[sub 3] at temperatures close to the critical temperature for amorphization. Journal of Applied Physics, 2006, 100, 113533.	1.1	25
418	Aluminum Nitride-Silicon Carbide Alloy Crystals Grown on SiC Substrates by Sublimation. MRS Internet Journal of Nitride Semiconductor Research, 2005, 10, 1.	1.0	6
419	Supercritical fluid immersion deposition: a new process for selective deposition of metal films on silicon substrates. Surface and Coatings Technology, 2005, 190, 25-31.	2.2	12
420	Surface electronic properties and site-specific laser desorption processes of highly structured nanoporous MgO thin films. Surface Science, 2005, 593, 242-247.	0.8	14
421	Iron oxide–gold core–shell nanoparticles and thin film assembly. Journal of Materials Chemistry, 2005, 15, 1821.	6.7	211
422	Thiophene hydrodesulfurization over nickel phosphide catalysts: effect of the precursor composition and support. Journal of Catalysis, 2005, 231, 300-313.	3.1	313
423	Erosion rate variations during XPS sputter depth profiling of nanoporous films. Surface and Interface Analysis, 2005, 37, 417-423.	0.8	11
424	Hydrogen bubbles and formation of nanoporous silicon during electrochemical etching. Surface and Interface Analysis, 2005, 37, 555-561.	0.8	7
425	Simple method for estimating and comparing x-ray damage rates. Journal of Vacuum Science and Technology A: Vacuum, Surfaces and Films, 2005, 23, 1740-1744.	0.9	5
426	Adsorption and Reaction of Methanol on Stoichiometric and Defective SrTiO3(100) Surfaces. Journal of Physical Chemistry B, 2005, 109, 4507-4513.	1.2	27
427	Nanoscale effects on ion conductance of layer-by-layer structures of gadolinia-doped ceria and zirconia. Applied Physics Letters, 2005, 86, 131906.	1.5	168
428	Monodispersed Coreâ^'Shell Fe3O4@Au Nanoparticles. Journal of Physical Chemistry B, 2005, 109, 21593-21601.	1.2	545
429	Gold–polyaniline composites : Part II. Effects of nanometer sized particles. Physical Chemistry Chemical Physics, 2005, 7, 3619.	1.3	42
430	Effects of Reduction Temperature and Metalâ `Support Interactions on the Catalytic Activity of Pt/γ-Al2O3 and Pt/TiO2 for the Oxidation of CO in the Presence and Absence of H2. Journal of Physical Chemistry B, 2005, 109, 23430-23443.	1.2	159
431	Functionalized TiO2Nanoparticles for Use for in Situ Anion Immobilization. Environmental Science & Technology, 2005, 39, 7306-7310.	4.6	45
432	Adsorption and Reaction of CO and CO2on Oxidized and Reduced SrTiO3(100) Surfaces. Journal of Physical Chemistry B, 2005, 109, 10327-10331.	1.2	48

#	Article	IF	CITATIONS
433	Relationship between the structural and magnetic properties of Co-dopedSnO2nanoparticles. Physical Review B, 2005, 72, .	1.1	250
434	ZnO nanoclusters: Synthesis and photoluminescence. Applied Physics Letters, 2005, 87, 241917.	1.5	49
435	Development of high-temperature ferromagnetism inSnO2and paramagnetism in SnO by Fe doping. Physical Review B, 2005, 72, .	1.1	204
436	Adsorptive Removal of Organic Sulfur Compounds from Jet Fuel over K-Exchanged NiY Zeolites Prepared by Impregnation and Ion Exchange. Industrial & Engineering Chemistry Research, 2005, 44, 5740-5749.	1.8	106
437	X-ray Photoelectron Spectroscopy Studies of Oxidized and Reduced Ce0.8Zr0.2O2(111) Surfaces. Surface Science Spectra, 2004, 11, 82-90.	0.3	1
438	X-ray Photoelectron Spectroscopy Studies of Oxidized and Reduced CeO2(111) Surfaces. Surface Science Spectra, 2004, 11, 73-81.	0.3	43
439	Direct determination of volume changes in ion-beam-irradiated SiC. Journal of Applied Physics, 2004, 95, 4687-4690.	1.1	32
440	Probing cation antisite disorder inGd2Ti2O7pyrochlore by site-specific near-edge x-ray-absorption fine structure and x-ray photoelectron spectroscopy. Physical Review B, 2004, 70, .	1.1	32
441	Room-temperature ferromagnetism in ion-implanted Co-doped TiO2(110) rutile. Applied Physics Letters, 2004, 84, 4466-4468.	1.5	49
442	Electrophilic Aromatic Substitutions of Amine and Sulfonate onto Fine-Grained Activated Carbon for Aqueous-Phase Metal Ion Removal. Separation Science and Technology, 2004, 39, 3263-3279.	1.3	21
443	Epitaxial growth and properties of cobalt-dopedZnOonαâ^'Al2O3single-crystal substrates. Physical Review B, 2004, 70, .	1.1	175
444	Spectroscopic Characterizations of Molecularly Linked Gold Nanoparticle Assemblies upon Thermal Treatment. Langmuir, 2004, 20, 4254-4260.	1.6	32
445	Reaction of hydroquinone with hematite. Journal of Colloid and Interface Science, 2004, 274, 433-441.	5.0	35
446	Adsorption and Reaction of Acetaldehyde on Stoichiometric and Defective SrTiO3(100) Surfaces. Journal of Physical Chemistry B, 2004, 108, 1646-1652.	1.2	16
447	Chemical Processing in High-Pressure Aqueous Environments. 7. Process Development for Catalytic Gasification of Wet Biomass Feedstocks. Industrial & Engineering Chemistry Research, 2004, 43, 1999-2004.	1.8	103
448	Noncovalent Functionalization of Carbon Nanotubes with Molecular Anchors Using Supercritical Fluidsâ€. Journal of Physical Chemistry B, 2004, 108, 8737-8741.	1.2	44
449	Supercritical fluid synthesis and characterization of catalytic metal nanoparticles on carbon nanotubes. Journal of Materials Chemistry, 2004, 14, 908.	6.7	246
450	Composition-Controlled Synthesis of Bimetallic Goldâ^'Silver Nanoparticles. Langmuir, 2004, 20, 11240-11246.	1.6	125

#	Article	IF	CITATIONS
451	X-ray photoelectron spectroscopic analyses of corrosion products formed on rock bolt carbon steel in chloride media with bicarbonate and silicate ions. Corrosion Science, 2004, 46, 2629-2649.	3.0	25
452	Redox properties of water on the oxidized and reduced surfaces of CeO2. Surface Science, 2003, 526, 1-18.	0.8	376
453	Oxidation of H2S by Iron Oxides in Unsaturated Conditions. Environmental Science & Technology, 2003, 37, 2192-2199.	4.6	55
454	Immersion Deposition of Metal Films on Silicon and Germanium Substrates in Supercritical Carbon Dioxide. Chemistry of Materials, 2003, 15, 83-91.	3.2	39
455	X-ray Photoelectron Spectroscopic Study of the Activation of Molecularly-Linked Gold Nanoparticle Catalysts. Langmuir, 2003, 19, 125-131.	1.6	93
456	Investigation of Copper(I) Oxide Quantum Dots by Near-Edge X-ray Absorption Fine Structure Spectroscopy. Chemistry of Materials, 2003, 15, 3939-3946.	3.2	21
457	Temperature-induced phase separation in chromium films. Applied Physics Letters, 2003, 82, 2230-2232.	1.5	11
458	Beam Damage of Poly(2-chloroethyl methylacrylate) [PCEMA] Films as Observed by X-ray Photoelectron Spectroscopy at 143 K, 303 K, and 373 K. Surface Science Spectra, 2003, 10, 80-100.	0.3	5
459	High energy ion beam studies of ion exchange in a Na2O–Al2O3–SiO2 glass. Journal of Applied Physics, 2002, 91, 1910-1920.	1.1	11
460	Performance of bare and sol-gel-coated DKDP crystal surfaces exposed to multiple 351-nm laser pulses in vacuum and air. , 2002, , .		4
461	Characterizations of Core-Shell Nanoparticle Catalysts for Methanol Electrooxidation. Materials Research Society Symposia Proceedings, 2002, 756, 1.	0.1	2
462	Evidence for Localization of Reaction upon Reduction of Carbon Tetrachloride by Granular Iron. Langmuir, 2002, 18, 7688-7693.	1.6	39
463	XAS and XPS Characterization of Monolayers Derived from a Dithiol and Structurally Related Disulfide-Containing Polyamides. Langmuir, 2002, 18, 8123-8128.	1.6	47
464	Surface decontamination of simulated chemical warfare agents using a nonequilibrium plasma with off-gas monitoring. IEEE Transactions on Plasma Science, 2002, 30, 1454-1459.	0.6	17
465	Interfacial chemistry and the performance of bromine-etched CdZnTe radiation detector devices. IEEE Transactions on Nuclear Science, 2002, 49, 2005-2009.	1.2	45
466	Electronic structure of ytterbium-doped strontium fluoroapatite: Photoemission and photoabsorption investigation. Journal of Applied Physics, 2002, 91, 5135-5140.	1.1	8
467	Use and limitations of electron flood gun control of surface potential during XPS: two non-homogeneous sample types. Surface and Interface Analysis, 2002, 33, 781-790.	0.8	63
468	In2O3/Al2O3 Catalysts for NOx Reduction in Lean Condition. Journal of Catalysis, 2002, 210, 97-105.	3.1	63

#	Article	IF	CITATIONS
469	Practical Aspects of Charging Phenomena in XPS as Demonstrated in Oxidized-Al Films on Al and Al Alloys. Journal of Surface Analysis (Online), 2002, 9, 396-403.	0.1	9
470	Selective Sorption of Cesium Using Self-Assembled Monolayers on Mesoporous Supports. Environmental Science & Technology, 2001, 35, 3962-3966.	4.6	168
471	The structure of Na2O–Al2O3–SiO2 glass: impact on sodium ion exchange in H2O and D2O. Journal of Non-Crystalline Solids, 2001, 296, 10-26.	1.5	142
472	Infrared transparent spinel films with p-type conductivity. Thin Solid Films, 2001, 398-399, 45-52.	0.8	140
473	Porous Silicon as a Versatile Platform for Laser Desorption/Ionization Mass Spectrometry. Analytical Chemistry, 2001, 73, 612-619.	3.2	337
474	Analyzing localized corrosion in lon-implanted metals via XPS/AES. Jom, 2001, 53, 37-41.	0.9	2
475	Chemical sensors based on dielectric response of functionalized mesoporous silica films. Journal of Materials Research, 2001, 16, 2810-2816.	1.2	54
476	Plasma etching of lead germanate (PGO) ferroelectric thin film. Journal of Vacuum Science and Technology A: Vacuum, Surfaces and Films, 2001, 19, 1341-1345.	0.9	3
477	First step towards the growth of single-crystal oxides on Si: Formation of a two-dimensional crystalline silicate on Si(001). Applied Physics Letters, 2001, 79, 3591-3593.	1.5	60
478	Approach for determining area selectivity in small-area XPS analysis. Surface and Interface Analysis, 2000, 29, 766-772.	0.8	22
479	MOCVD growth and structure of Nb- and V-doped TiO2 films on sapphire. Journal of Crystal Growth, 2000, 212, 178-190.	0.7	57
480	Effectiveness of high energy ion beam techniques for the characterization of mesoporous low dielectric-constant materials. Nuclear Instruments & Methods in Physics Research B, 2000, 161-163, 476-481.	0.6	0
481	Third Row Transition Metals by X-ray Photoelectron Spectroscopy. Surface Science Spectra, 2000, 7, 1-68.	0.3	31
482	Interaction of HCOOH with stoichiometric and reduced SrTiO3(100) surfaces. Journal of Vacuum Science and Technology A: Vacuum, Surfaces and Films, 2000, 18, 1893-1899.	0.9	10
483	Surfaces with Reversible Hydrophilic/Hydrophobic Characteristics on Cross-linked Poly(N-isopropylacrylamide) Hydrogels. Langmuir, 2000, 16, 8016-8023.	1.6	102
484	The Microstructure, Phase and Ferroelectric Properties of PZT Thin Films on Oriented Multilayer Electrodes. Materials Research Society Symposia Proceedings, 1999, 596, 199.	0.1	4
485	Corrosion of Phosphorusâ€Implanted 304L Stainless Steel in 1 N  H 2 SO 4. Journal of the Elec Society, 1999, 146, 984-987.	rtrochemio	cal 1
486	Vacuum Cleaved Calcium Carbonate by XPS. Surface Science Spectra, 1999, 6, 153-159.	0.3	12

#	Article	IF	CITATIONS
487	The ion beam materials analysis laboratory at the environmental molecular sciences laboratory. Nuclear Instruments and Methods in Physics Research, Section A: Accelerators, Spectrometers, Detectors and Associated Equipment, 1999, 420, 81-89.	0.7	64
488	Interactions of liquid and vapor water with stoichiometric and defective TiO2(100) surfaces. Surface Science, 1999, 440, 60-68.	0.8	35
489	Electrochemistry of TiN in 6 M KOH Solution. Journal of the Electrochemical Society, 1998, 145, 1211-1218.	1.3	27
490	Comparative SHG and XPS studies of interactions between defects and N2O on rutile TiO2(110) surfaces. Surface Science, 1997, 392, 1-7.	0.8	30
491	Interactions of HCOOH with stoichiometric and defective TiO2(110) surfaces. Surface Science, 1997, 380, 352-364.	0.8	90
492	Structure of the cleaved CaCO3(101̄4) surface in an aqueous environment. Surface Science, 1996, 351, 172-182.	0.8	114
493	Nucleophilic Displacements in Mixed Self-Assembled Monolayersâ€. Langmuir, 1996, 12, 5064-5075.	1.6	136
494	The Interaction of Liquid and Vapor Water with Nearly Defect-Free and Defective TiO2(100) Surfaces. Materials Research Society Symposia Proceedings, 1996, 432, 45.	0.1	1
495	Comparative second harmonic generation and X-ray photoelectron spectroscopy studies of the UV creation and O2 healing of Ti3+ defects on (110) rutile TiO2 surfaces. Surface Science, 1995, 339, 114-124.	0.8	140
496	The adsorption of liquid and vapor water on TiO2(110) surfaces: the role of defects. Surface Science, 1995, 344, 237-250.	0.8	228
497	Creation of variable concentrations of defects on TiO2(110) using low-density electron beams. Surface Science, 1994, 320, 295-306.	0.8	148
498	Spatially Resolved Mineral Deposition on Patterned Self-Assembled Monolayers. Langmuir, 1994, 10, 619-622.	1.6	97
499	The Adsorption of Liquid and Vapor Water on TiO ₂ (110) Surfaces: The Role of Defects. Materials Research Society Symposia Proceedings, 1994, 357, 97.	0.1	2
500	Beam damage of selfâ€assembled monolayers. Journal of Vacuum Science and Technology A: Vacuum, Surfaces and Films, 1993, 11, 2292-2297.	0.9	54
501	Biomimetic Lithography and Deposition Kinetics of Iron Oxyhydroxide Thin Films. Materials Research Society Symposia Proceedings, 1993, 330, 139.	0.1	1
502	Influence of adsorbed and implanted sulfur on the corrosion of iron in calcium nitrate at 60 °C. Journal of Vacuum Science and Technology A: Vacuum, Surfaces and Films, 1992, 10, 3007-3011.	0.9	5
503	Fractal character of crack propagation in epoxy and epoxy composites as revealed by photon emission during fracture. Journal of Materials Research, 1991, 6, 183-195.	1.2	28
504	Reaction of soda lime silicate glass in isotopically labelled water. Journal of Non-Crystalline Solids, 1986, 86, 369-380.	1.5	40

#	Article	IF	CITATIONS
505	Characterization of ferromagnetic Co-implanted rutile TiO/sub 2/(110). , 0, , .		0
506	Enabling High-Voltage Lithium Metal Batteries Under Practical Conditions. SSRN Electronic Journal, 0,	0.4	0